Energy Harvesting For The Internet-of-Things: Measurements And Probability Models

George Smart, John Atkinson, John Mitchell, Miguel Rodrigues and Yiannis Andreopoulos

Dept. of Electronic and Electrical Engineering

University College London

London, UK

{george.smart, john.atkinson.10, j.mitchell, m.rodrigues, i.andreopoulos}@ucl.ac.uk

Abstract—**The success of future Internet-of-Things (IoT) based application deployments depends on the ability of wireless sensor platforms to sustain uninterrupted operation based on environmental energy harvesting. In this paper, we deploy a multi-transducer platform for photovoltaic and piezoelectric energy harvesting and collect raw data about the harvested power in commonly-encountered outdoor and indoor scenarios. We couple the generated power profiles with probability mixture models and make our data and processing code freely available to the research community for wireless sensors and IoT-oriented applications. Our aim is to provide data-driven probability models that characterize the energy production process, which will substantially facilitate the coupling of energy harvesting statistics with energy consumption models for processing and transceiver designs within upcoming IoT deployments.**

Index Terms—**energy harvesting, experimental testbeds, Internet-of-Things, wireless sensor networks**

I. INTRODUCTION

ENERGY HARVESTING is now recognized as an important aspect of wireless sensor networks (WSNs) and Internet-of-Things (IoT) oriented technologies [1]. Indeed, a multitude of research efforts have studied energy management policies [2], theoretical aspects of coupling energy production with energy consumption [3], and practical applications [1], [4]. While most manufacturers of transducers provide specifications for the minimum, maximum and average energy harvesting characteristics of their devices, (photovoltaic, piezo-electric, thermoelectric, etc.), there is still a significant gap between the reality of practical energy harvesting testbeds and the assumptions made in the research literature. For example, within the recent literature on energy-harvesting based communications, there is a flurry of probability models about the harvesting process [5], but very limited experimental evidence is provided to support such models. This can be seen as a bottleneck in advancing the state-of-the-art in energy management frameworks for WSNs and IoT applications, as well as limiting the applicability and impact of theoretical studies in the field.

In this work, we attempt to provide an initial coverage of this gap by providing measurements and associated software tools to capture, parse and model photovoltaic and piezo-electric energy harvesting with a real-world multi-transducer platform. Our focus is on the "raw" power produced by each transducer after power conditioning, as measured by high-frequency analog-to-digital (ADC) conversion that causes no interference on the actual harvesting process. The selected application environments are an outdoor and two indoor environments that represent typical office and residential conditions where IoT-based applications and devices are expected to operate. The derived experimental datasets are matched with a variety of scaled probability distribution functions and results from the best-fit for each case are provided. Based on our results, we show that, for all our experiments, a mixture of two to four Normal and Half-Normal distributions turns out to provide for the best fit for all cases under consideration. It is hoped that future energy management frameworks will make use of our results in order to optimize the link between energy production and consumption in IoT-oriented deployments.

Section II provides a summary of related work. Section III presents the data collection process. Section IV presents the results and corresponding probability models. Finally, Section V provides some concluding remarks.

II. RELATED WORK

The literature on energy harvesting approaches for wireless sensors and IoT-oriented platforms can broadly be separated in three categories. The first category relates to physical properties and design of transducer technologies that scavenge energy from the environment. Essentially, the available sources of energy are: light, radio-frequency (RF), electromagnetic radiation, thermal gradients and motion (including fluid flow). The focus of research work in this category is on physical design of harvesters and transducing rates, rather than the statistical characterization of the manner energy is produced across time and within different environmental conditions. From the reported results for the transducer technologies available for the four sources of environmental energy, the most mature and commercially available ones are solar cells and piezoelectric energy harvesters [4], [6]–[10]. Ambient RF, electromagnetic radiation and thermal gradients have also received some attention (e.g., the Seiko thermic watch), but the availability of significant power levels is an issue, and, for the case of RF, efficient extraction using devices much smaller than the radiation wavelength is another key challenge [7]. Beyond these energy sources, fuel-based generation using ambient fluids, such as human bodily fluids, has also been reported [7]. Overall, the general consensus from the related literature [4], [6]–[10] is that piezoelectric and photovoltaic

energy transducers are the most versatile and commercially mature technologies to consider for WSN and IoT-oriented deployments.

The second literature category relates to energy management frameworks for energy-harvesting based communications frameworks [2], [3], [5], [11]. Work in this area essentially tries to couple energy production and energy consumption in order to prolong the lifetime of particular sensing and communications platforms. Several frameworks have been proposed, which depend on the availability and characteristics of energy storage on the IoT devices, as well as on the statistical properties of the manner energy is being produced and consumed [10], [12]–[15]. While there is already a body of work on statistical characterization of energy consumption of transceivers and processor designs in several application domains [3], [5], [10], [12], [13], [15], the general consensus is that data-driven statistical characterization of energy harvesting requires more experimental evidence from practical testbeds, which is indeed the motivation for our work in this paper.

Finally, the last category of research relates to information-theoretic characterizations (typically in the form of upper or lower bounds) of the achievable data throughput and data processing capability in function of the energy harvesting statistics [5]. Again, a major gap in this domain is the validation of the statistical models for the assumed energy production processes based on real data. Therefore, we find that the experiments and statistical models of this work complement and provide empirical evidence that will be of use in all of these categories.

III. DATA COLLECTION PLATFORM & METHODOLOGY

This section provides details of the hardware and software platform used to collect empirical measurements of harvested energy available in several scenarios. Beyond the description of this report, we document and provide the source code used for our measurements, as well as the full set of measurements, at the experiment website: http://github.com/m1geo/EH_IOT.

1) Energy Harvesting: To provide the energy harvesting part of the hardware platform we used a Linear Technology (LT) DC2042A energy harvesting multisource demo board. As detailed in Table I, this board allows for energy harvesting from a variety external of transducers via a single compact circuit board, with transducers co-located in an easily accessible configuration.

Connected to this demo board are the energy harvesting transducer components, which operate as described in Table II. In addition, the platform provides a light sensor to measure ambient light levels in Lux, thereby adding context to the levels of solar energy harvested. The board and its associated components are shown in Fig. 1.

2) Portable Data Logger: The LT DC2042A harvesting board is capable of harvesting, storing and managing the power supply to low-power hardware suitable for wireless sensor network and Internet-of-Things oriented applications. For our measurement scenario, we are interested in the non-buffered "raw" power output from each individual harvesting scheme in Table II. Since each of the power outputs could be
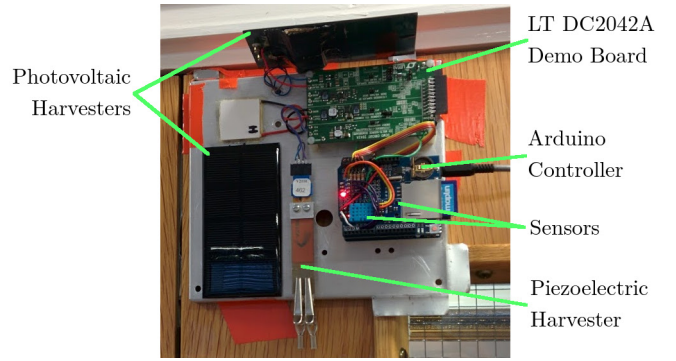

Figure 1. Energy harvesting platform with annotations on key components.

designated to support a sensor mote, we emulate a constant load using an accurate, carefully selected resistor. The resistor causes current to flow, thus dissipating energy. By attaching the DC2042A outputs to the analogue inputs of an Arduino Uno (an open source electronics prototyping platform) and using the Arduino's built-in 10-bit analogue to digital converters (ADCs), periodic samples that measure the energy dissipated into the resistor are captured for each of the individual harvesting schemes. These samples are deliberately captured without the use of any "power supervisor" ICs that would store, regulate and combine the harvested energy in order to support an attached device. This deliberate "raw" sampling allows the energy available from each source to be recorded and analysed separately and accurately. The Arduino runs a custom C routine that samples the energy harvested from the different schemes, as well as the light and temperature sensors, every 100 milliseconds. The samples are written to an SD card using comma separated values (CSVs) and a standard FAT32 file system for off-line analysis using Matlab. Since the Arduino is used solely as a monitoring & logging device and draws power from an external power source (mains supply or external battery), it is a passive measurement device and does not affect our experiment beyond the selection of sampling frequency and ADC accuracy.

A. Experimental Scenarios

This section details the environments where our data collection was performed. First, we remark that the core energy harvesting platform remains unchanged between scenarios. During outdoors experiments, the platform was enclosed in a waterproof housing that allowed for unimpeded movement of the piezoelectric harvester, and did not obscure light to on the photovoltaic panels or ambient light sensor. However, the piezoelectric harvester's physical resonance is tuned to a frequency appropriate to each individual scenario by adjusting the mass attached to it in accordance with the piezoelectric harvester datasheet [16]. Similarly, each of the load resistances are altered independently to match the energy available for each scenario (see Table III-A). These tuning techniques attempt to: *(i)* maximise the energy harvesting efficiency according to the ambient environment, and *(ii)* allow the testbed to record the best dynamic range for the harvester output.

Table I
LINEAR TECHNOLOGY DC2042A ENERGY HARVESTING MULTISOURCE DEMO BOARD COMPONENTS.

	Part Name	Purpose	IC No.
A	10V Micropower Synchronous Boost Converter	Solar Energy Harvesting	LTC3459
B	Piezoelectric Energy Harvesting Power Supply	Piezoelectric Energy Harvesting	LTC3588-1
C	Ultralow Voltage Step-Up Converter and Power Manager	Thermal Differential Energy Harvesting *(unused)*	LTC3108
D	Step-Up DC/DC Converter with Power Point Control & Low Drop Out Regulator	Misc. DC Energy Harvesting *(unused)*	LTC3105
E	Ultralow Power Supervisor with Power-Fail Output Selectable Thresholds	Supervises supply to connected device *(unused)*	LTC2935-2

Table II
TEST BED COMPONENTS COMPONENTS.

Transducer	Description	Part	Connects to...
Photovoltaic	Harvests light. Two panels in series consisting of 16 x $2.5cm^2$ cells. Total area $40cm^2$.	Sol SM2380	EH Board A
Piezoelectric	Harvests vibration. Attached mass and resonant frequency varied per scenario.	Mide V21BL	EH Board B
Light sensor	16-bit ambient light sensor measures light fall on photovoltaic panels	ROHM BH1750	Arduino

Table III
SCENARIO LOAD RESISTANCES.

Scenario	Office Door	Roof Ledge	Car Trunk
Photovoltaic	7.19 kΩ	4.67 kΩ	7.19 kΩ
Piezoelectric	42.2 kΩ	42.2 kΩ	42.2 kΩ

1) Office door: In the office door scenario, the testbed was firmly affixed with metal brackets to the door of a ~ 15 person research office. The office is primarily occupied between 7am-11pm with majority of activity between 10am-8pm during weekdays, with little activity during weekends. The office is lit by a mixture of natural sunlight during daylight hours, as well as standard office fluorescent lamps when the office is occupied. The office door automatically closes with reasonable force after every opening due to a spring-operated mechanism, as commonly found within office buildings for fire safety and security.

2) Roof ledge: For this scenario, the testbed was affixed securely to an outside roof ledge on an 11th floor window of the University College London Roberts Building. The building is located in central London, with the testbed being approximately 50m above the ground. In this scenario, a simple wind-sail of area of (approximately) $250cm^2$ was attached to the piezoelectric harvester via a stiff but lightweight aluminium connecting rod. This enables us to catch gusts of wind commonly observed on rooftops, as well as low frequency vibrations caused by the turbulence of steady wind movement around the sail. For the duration of the experiment, the temperature was recorded at an average 18°C during daylight hours, with an average wind speed of 6 km/h, gusting to 25 km/h. The sky was noted as mostly clear, but with some occasional cloud cover[1].

3) Car trunk: This scenario saw the testbed strapped securely into the trunk of a large family car. The piezoelectric harvester was tuned to 35 Hz to match the peak of vibration for a vehicle. The drive was largely on well-maintained tarmac roads (UK highways) at the speed limit (120 km/h), causing a constant vibration of around 40 Hz. Some of the journey was over rough terrain, causing a much more random frequency distribution and more intense oscillation of the piezoelectric transducer. Although the trunk was not completely sealed from light, inside of the trunk is covered by a parcel-shelf so minimal ambient light reached the harvester. Since the journey was made at night, the main sources of light were motorway lighting and moonlight.

IV. DATA ANALYSIS & VISUALISATION

Analysis and visualisation work was performed using Matlab. As with the Arduino program, the code to generate these model fittings and figures from the Arduino CSV data files is made available on the experiment's dedicated website: http://github.com/m1geo/EH_IOT.

A. Data Preparation

Voltage sample data are imported from the Arduino via CSV files, which are loaded into Matlab. From the voltage samples, power can calculated using Ohm's law, giving instantaneous energy dissipation readings at regular time intervals. The data is trimmed to retain only the active periods; periods of 5 minutes and longer with no harvesting are removed - examples are during dark periods for photovoltaic and periods without movement for piezoelectric. Graph fits were computed by approximating a fit manually and then exhaustively searching for the optimal fit to minimise the Kullback–Leibler (KL) divergence, D_{KL}, given by

$$D_{\text{KL}} = \sum_n P(n) \log_2 \frac{P(n)}{Q(n)} \tag{1}$$

with P the theoretical probability distribution under consideration and Q the experimentally-measured (and normalized) histogram of energy values sampled at points n.

---

[1] At the time of this writing, full weather conditions for the day are available here:
http://www.wunderground.com/personal-weather-station/dashboard?ID=IGREATER13#history/s20150530/e20150530/mdaily

B. Empirical Observations and Models under Consideration

Table IV shows mean and maximum energy values obtained for each of the three scenarios under consideration. Evidently, the three scenarios under consideration represent different cases for each modality of energy harvesting. For example, the "Car trunk" scenario represents the low-end of the harvesting spectrum, where both photovoltaic and piezoelectric power is modest. The indoors "Office door" scenario represents the mid-range scenario where medium photovoltaic and moderate piezoelectric harvesting is achievable. Finally, the outdoors "Roof ledge" scenario represents the most volatile case where, on average, high photovoltaic and piezoelectric powers can be harvested.

In terms of modeling, we considered mixture models of several distributions, including Exponential, inverse-Gamma, Normal, Half-Normal, Poisson and Pareto. Out of a multitude of fitting experiments via the minimization of (1), mixtures using the following two distributions were found to provide for the best results:

- the Normal distribution with mean μ and standard deviation σ:

$$P_{\mathrm{N}}(\mu, \sigma) = \frac{1}{\sigma\sqrt{2\pi}} e^{\frac{-(x-\mu)^2}{2\sigma^2}} \qquad (2)$$

- the Half-Normal distribution with mean $\sigma\sqrt{\frac{2}{\pi}}$ and standard deviation $\sigma\sqrt{1 - \frac{2}{\pi}}$:

$$P_{\mathrm{HN}}(\sigma) = \frac{\sqrt{2}}{\sigma\sqrt{\pi}} e^{\frac{-x^2}{2\sigma^2}} \qquad (3)$$

For each harvesting scenario, we also provide the associated scaling parameters, s, to normalize the experimentally-measured data to the theoretical probability distributions.

1) Office door:

a) Photovoltaic: For the case of photovoltaic harvesting, the best fit was obtained with a mixture of three Normal distributions. The resulting fit is shown in Fig. 2 and it corresponds to

$$\begin{aligned} P_{\mathrm{door,PV}} &= s_{\mathrm{door,PV}} \left[a_1 P_{\mathrm{N}}(\mu_1, \sigma_1) \right. \qquad (4)\\ &+ \left. a_2 P_{\mathrm{N}}(\mu_2, \sigma_2) + a_3 P_{\mathrm{N}}(\mu_3, \sigma_3) \right] \end{aligned}$$

with the parameters given in Table V and scaling factor $s_{\mathrm{door,PV}} = 6.076 \times 10^{-2}$. The KL divergence for this case was found to be: $D_{\mathrm{KL}} = 4.823 \times 10^{-2}$.

Table V
PHOTOVOLTAIC HARVESTER ON OFFICE DOOR.

i	a_i	μ_i	σ_i
1	5.038	1.541e-05	6.059e-06
2	7.582	3.022e-05	1.213e-05
3	6.943	1.779e-05	1.107e-04

b) Piezoelectric: For the case of piezoelectric harvesting, the best fit was obtained with a mixture of two Half-Normal and one Normal distribution. The resulting fit is shown in Fig. 3 and it corresponds to

$$\begin{aligned} P_{\mathrm{door,PE}} &= s_{\mathrm{door,PE}} \left[a_1 P_{\mathrm{HN}}(\sigma_1) \right. \qquad (5)\\ &+ \left. a_2 P_{\mathrm{HN}}(\sigma_2) + a_3 P_{\mathrm{N}}(\mu_3, \sigma_3) \right] \end{aligned}$$
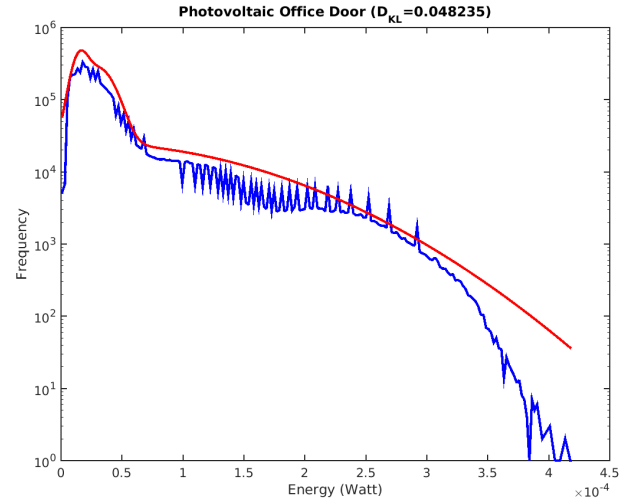

Figure 2. Histogram of photovoltaic harvester (blue) on "Office door" and best fit (red) obtained via (4).

with the parameters given in Table VI and scaling factor $s_{\mathrm{door,PE}} = 613.787 \times 10^{-2}$. The KL divergence for this case was found to be: $D_{\mathrm{KL}} = 1.081 \times 10^{-2}$.
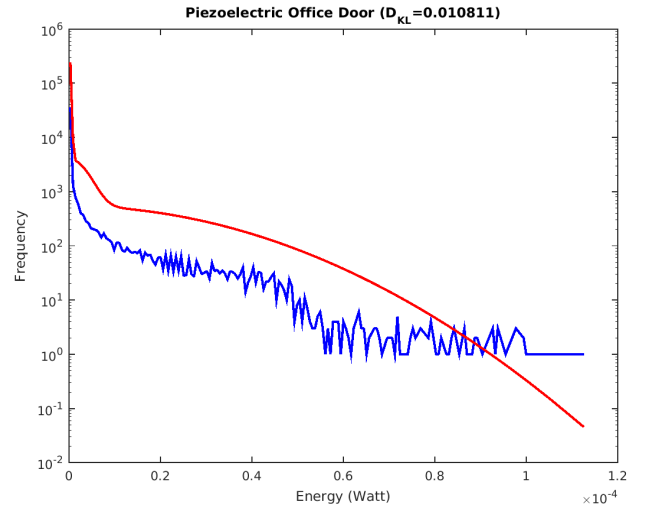

Figure 3. Histogram of piezoelectric harvester (blue) on "Office door" and best fit (red) obtained via (5).

Table VI
PIEZOELECTRIC HARVESTER ON OFFICE DOOR.

i	a_i	μ_i	σ_i
1	1.306e-01	0	2.894e-07
2	1.471e-02	0	3.384e-06
3	3.522e-02	4.867e-09	2.598e-05

2) Roof ledge:

a) Photovoltaic: For the case of photovoltaic harvesting, the best fit for the "Roof ledge" experimental data was obtained with a mixture of three Normal distributions and one

Table IV
EMPIRICAL SCENARIO CONDITIONS. VALUES REPORTED ARE AVERAGE, WITH MAXIMA IN BRACKETS. ALL MINIMA ARE ZERO.

Scenario	Ambient Light (Lux)	Photovoltaic Power (μW)	Piezoelectric Power (μW)
Office door	56.47 (231)	41.15 (418.7131)	2.43 (112.6020)
Roof ledge	5697.10 (54612)	953.58 (2422.857)	6.38 (133.1557)
Car trunk	1.30 (370)	7.97 (1563.537)	5.32 (156.6202)

Half-Normal distribution. The resulting fit is shown in Fig. 4 and it corresponds to

$$P_{\text{roof,PV}} = s_{\text{roof,PV}} \left[a_1 P_{\text{HN}}(\sigma_1) + a_2 P_{\text{N}}(\mu_2, \sigma_2) \right. \tag{6}$$
$$\left. + a_3 P_{\text{N}}(\mu_3, \sigma_3) + a_4 P_{\text{N}}(\mu_4, \sigma_4) \right]$$

with the parameters given in Table VII and scaling factor $s_{\text{roof,PV}} = 2.943 \times 10^{-2}$. The KL divergence for this case was found to be: $D_{\text{KL}} = 4.716 \times 10^{-2}$.
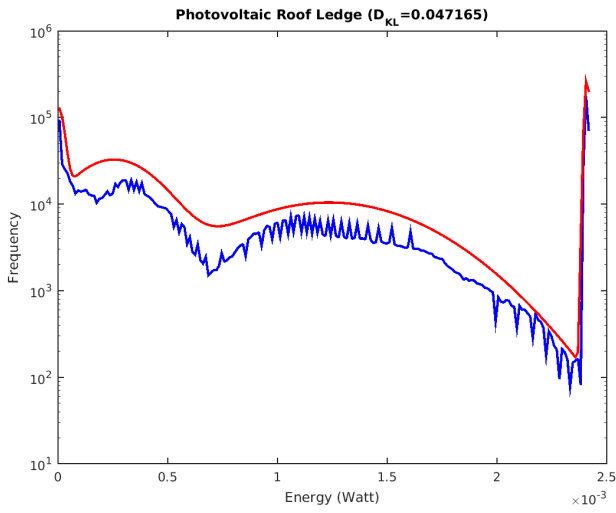

Figure 4. Histogram of photovoltaic harvester (blue) on "Roof ledge" and best fit (red) obtained via (6).

Table VII
PHOTOVOLTAIC HARVESTER ON ROOF LEDGE.

i	a_i	μ_i	σ_i
1	3.444	0	2.327e-05
2	14.626	2.517e-04	1.812e-04
3	10.230	1.234e-03	3.914e-04
4	6.888	2.409e-03	9.627e-06

b) Piezoelectric: For the case of piezoelectric harvesting, the best fit was obtained with a mixture of one Half-Normal and two Normal distributions. The resulting fit is shown in Fig. 5 and it corresponds to

$$P_{\text{roof,PE}} = s_{\text{roof,PE}} \left[a_1 P_{\text{HN}}(\sigma_1) \right. \tag{7}$$
$$\left. + a_2 P_{\text{N}}(\mu_2, \sigma_2) + a_3 P_{\text{N}}(\mu_3, \sigma_3) \right]$$

with the parameters given in Table VIII and scaling factor $s_{\text{roof,PE}} = 186.529 \times 10^{-2}$. The KL divergence for this case was found to be: $D_{\text{KL}} = 0.910 \times 10^{-2}$.
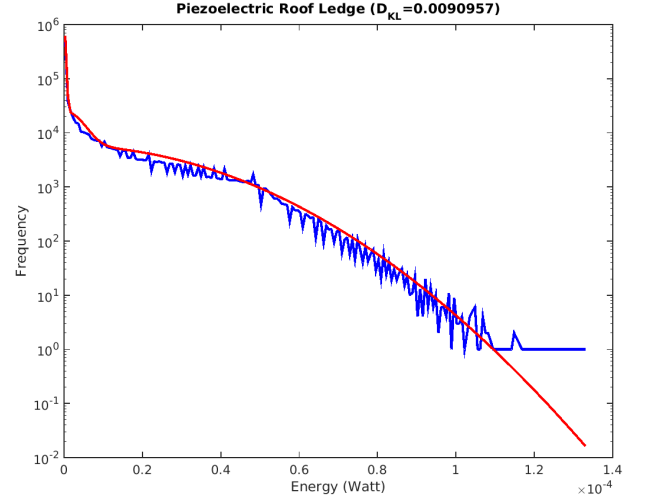
3) Car trunk:

Figure 5. Histogram of piezoelectric harvester (blue) on "Roof ledge" and best fit (red) obtained via (7).

Table VIII
PIEZOELECTRIC HARVESTER ON ROOF LEDGE.

i	a_i	μ_i	σ_i
1	3.915e-01	0	3.7025e-07
2	9.750e-02	9.971e-09	4.002e-06
3	1.915e-01	4.867e-09	2.631e-05

a) Photovoltaic: For the case of photovoltaic harvesting, the best fit for the "Car trunk" experimental data was obtained with a mixture of two Normal distributions and one Half-Normal distribution. The resulting fit is shown in Fig. 6 and it corresponds to

$$P_{\text{car,PV}} = s_{\text{car,PV}} \left[a_1 P_{\text{HN}}(\sigma_1) \right. \tag{8}$$
$$\left. + a_2 P_{\text{N}}(\mu_2, \sigma_2) + a_3 P_{\text{N}}(\mu_3, \sigma_3) \right]$$

with the parameters given in Table IX and scaling factor $s_{\text{car,PV}} = 71.332 \times 10^{-2}$. The KL divergence for this case was found to be: $D_{\text{KL}} = 0.777 \times 10^{-2}$.

Table IX
PHOTOVOLTAIC HARVESTER IN CAR TRUNK.

i	a_i	μ_i	σ_i
1	1.363	0	2.000e-06
2	4.170e-02	4.578e-09	3.691e-05
3	3.607e-02	1.075e-08	4.163e-04

b) Piezoelectric: Finally, for the case of piezoelectric harvesting, the best fit for the "Car trunk" experiment was obtained with a mixture of one Normal and two Half-Normal
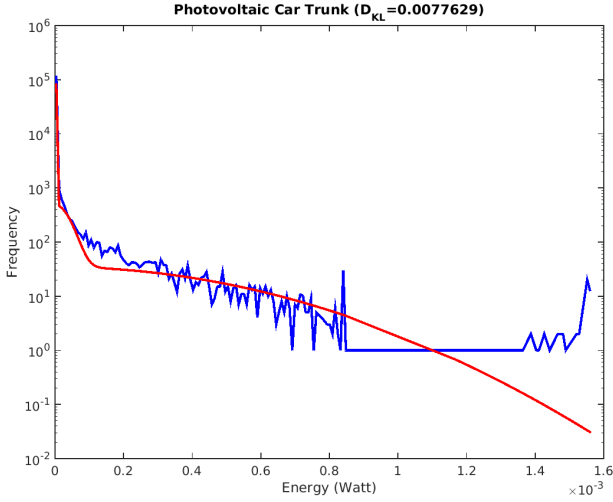
Figure 6. Histogram of photovoltaic harvester (blue) on "Car trunk" and best fit (red) obtained via (8).

distributions. The resulting fit is shown in Fig. 7 and it corresponds to

$$
\begin{aligned}
P_{\mathrm{car,PE}} = & \ s_{\mathrm{car,PE}} \left[a_1 P_{\mathrm{HN}}(\sigma_1) \right. \\
& \left. + \ a_2 P_{\mathrm{HN}}(\sigma_2) + a_3 P_{\mathrm{N}}(\mu_3, \sigma_3) \right]
\end{aligned}
\tag{9}
$$

with the parameters given in Table X and scaling factor $s_{\mathrm{car,PE}} = 1555.130 \times 10^{-2}$. The KL divergence for this case was found to be: $D_{\mathrm{KL}} = 3.431 \times 10^{-2}$.
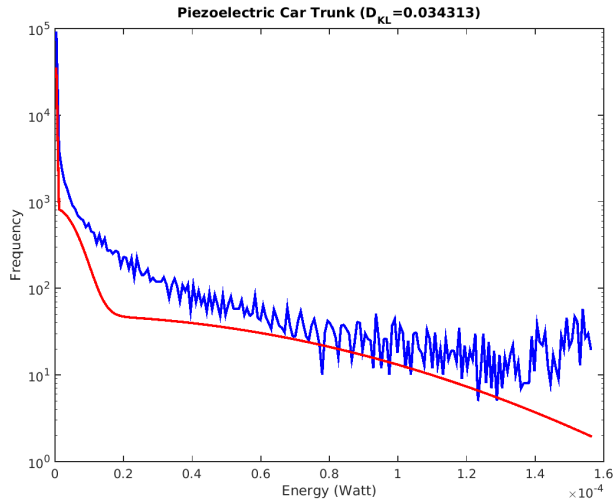

Figure 7. Histogram of piezoelectric harvester (blue) on "Car trunk" and best fit (red) obtained via (9).

Table X
PIEZOELECTRIC HARVESTER IN CAR TRUNK.

i	a_i	μ_i	σ_i
1	5.715e-02	0	2.000e-07
2	5.261e-03	0	5.351e-06
3	3.784e-03	4.867e-09	6.159e-05

V. CONCLUSION

Our work is motivated by the lack of experimental evidence on the capabilities of practical transducer technologies in scenarios appropriate to Internet-of-Things deployments. To complement this current gap of data and associated probability models, we deployed a multi-transducer platform for photovoltaic and piezoelectric energy harvesting, which are technologies that are expected to be deployed within IoT-oriented data gathering and transmission frameworks. The provided experiments and the associated online repository at http://github.com/m1geo/EH_IOT provide a full dataset that can be used for research in energy-neutral operation of IoT platforms, as well as feasibility studies in energy optimization of practical deployments, before engaging in cumbersome deployments in the field.

VI. ACKNOWLEDGEMENTS

REFERENCES

[1] J. Gubbi, R. Buyya, S. Marusic, and M. Palaniswami, "Internet of things (iot): A vision, architectural elements, and future directions," *Fut. Gen. Comp. Syst.*, vol. 29, no. 7, pp. 1645–1660, 2013.

[2] A. Kansal, J. Hsu, S. Zahedi, and M. B. Srivastava, "Power management in energy harvesting sensor networks," *ACM Trans. on Embed. Comp. Syst. (TECS)*, vol. 6, no. 4, p. 32, 2007.

[3] H. Besbes *et al.*, "Analytic conditions for energy neutrality in uniformly-formed wireless sensor networks," *IEEE Trans. Wireless Comm.*, vol. 12, no. 10, pp. 4916–4931, 2013.

[4] M. N. Halgamuge *et al.*, "An estimation of sensor energy consumption," vol. 12, pp. 259–295, 2009.

[5] S. Ulukus, A. Yener, E. Erkip, O. Simeone, M. Zorzi, P. Grover, and K. Huang, "Energy harvesting wireless communications: A review of recent advances," *IEEE. J. Select. Areas in Comm.*, vol. 33, no. 3, pp. 360–381, 2015.

[6] S. P. Beeby, M. J. Tudor, and N. White, "Energy harvesting vibration sources for microsystems applications," *Measurement science and technology*, vol. 17, no. 12, p. R175, 2006.

[7] P. D. Mitcheson *et al.*, "Energy harvesting from human and machine motion for wireless electronic devices," *Proc. of the IEEE*, vol. 96, no. 9, pp. 1457–1486, 2008.

[8] S. Roundy, D. Steingart, L. Frechette, P. Wright, and J. Rabaey, "Power Sources for Wireless Sensor Networks," *Sensor Networks*, vol. 2920, pp. 1–17, 2004. [Online]. Available: http://www.springerlink.com/index/B0UTGM8AHNPHLL3L.pdf

[9] V. Raghunathan *et al.*, "Design considerations for solar energy harvesting wireless embedded systems," in *Proc. 4th Int. Symp. Inf. Process. Sensor Networks*. IEEE Press, 2005, p. 64.

[10] S. Sudevakatam and P. Kulkarni, "Energy Harvesting Sensor Nodes: Survez and Implications," *IEEE Comm. Surv. and Tut.*, vol. 13, no. 3, pp. 443–461, 2011.

[11] P. N. Whatmough *et al.*, "A 0.6 v all-digital body-coupled wakeup transceiver for iot applications," in *Proc. IEEE Int. Symp. VLSI Circuits*. IEEE, 2015, pp. C98–C99.

[12] V. Sharma, U. Mukherji, V. Joseph, and S. Gupta, "Optimal energy management policies for energy harvesting sensor nodes," *IEEE Trans. Wireless Comm.*, vol. 9, no. 4, pp. 1326–1336, 2010.

[13] N. Kontorinis *et al.*, "Statistical framework for video decoding complexity modeling and prediction," *IEEE Trans. Circ. and Syst. for Video Technol.*, vol. 19, no. 7, pp. 1000–1013, 2009.

[14] B. Foo *et al.*, "Analytical rate-distortion-complexity modeling of wavelet-based video coders," *IEEE Trans. Signal Processing*, vol. 56, no. 2, pp. 797–815, 2008.

[15] Y. Andreopoulos and M. Van der Schaar, "Adaptive linear prediction for resource estimation of video decoding," *IEEE Trans. Circ. and Syst. for Video Technol.*, vol. 17, no. 6, pp. 751–764, 2007.

[16] MIDÉ. Volture piezoelectric energy harvesters datasheet. [Online]. Available: http://www.mide.com/pdfs/Volture_Datasheet_001.pdf